PEEM and XPEEM: methodology and applications for dynamic processes

PEEM methods and General considerations

- Chemical imaging
- Magnetic imaging
  - XMCD/XMLD
  - Examples
  - Dynamic studies

Why X-ray microscopy?

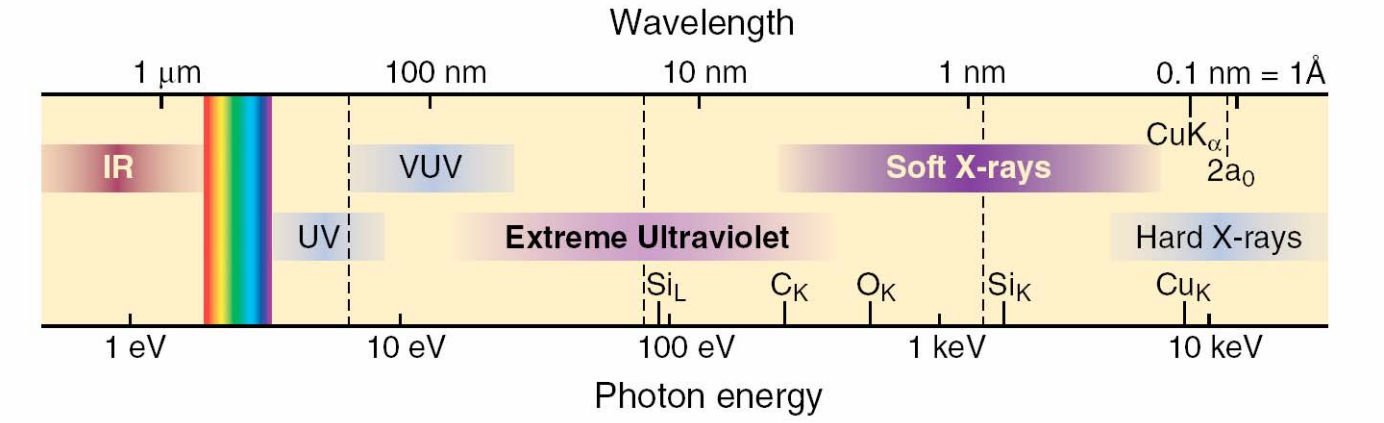

1. Combining *high spatial resolution* with intrinsic *chemical sensitivity* of X-rays
2. Chemical maps in 2D
3. Chemical maps in 3D (tomography)
4. Pulsed nature of SR for dynamic measurements

Instrumental approach

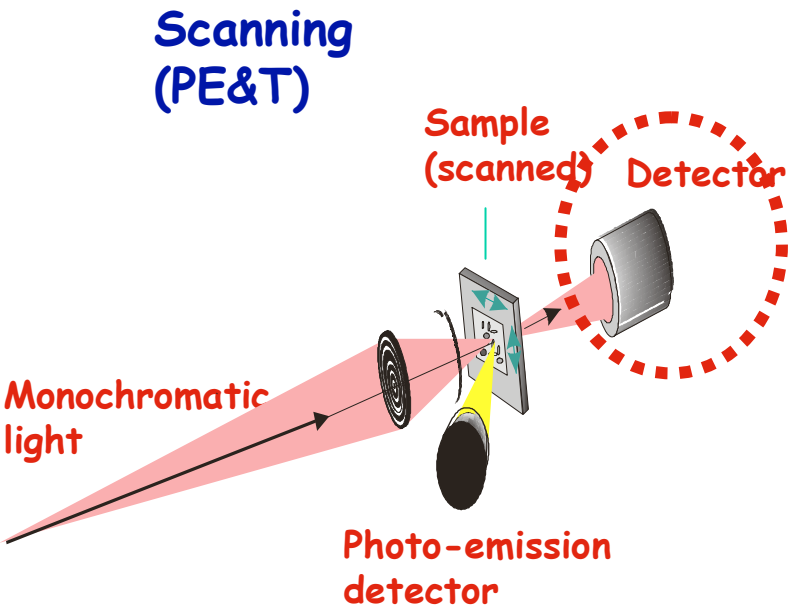

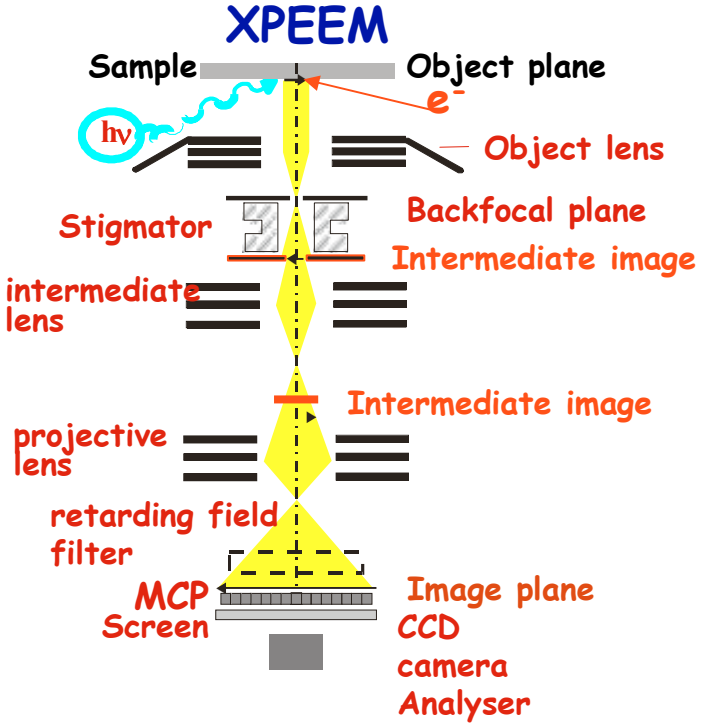

Photon optics is de-magnifying the beam:

Scanning Instrument

1. Whole power of XPS in a small spot mode.
2. Flexibility for adding different detectors.
3. Rough surfaces can be measured.
4. Limited use for fast dynamic processes.

Electron optics to magnify irradiated area:

Imaging Instrument

1. High lateral resolution (20 nm).
2. Multi-method instrument (XPEEM/PED).
3. Excellent for monitoring dynamic processes.
4. Poorer spectroscopic ability.
5. Sensitive to rough surfaces.

Contrast modes in PEM

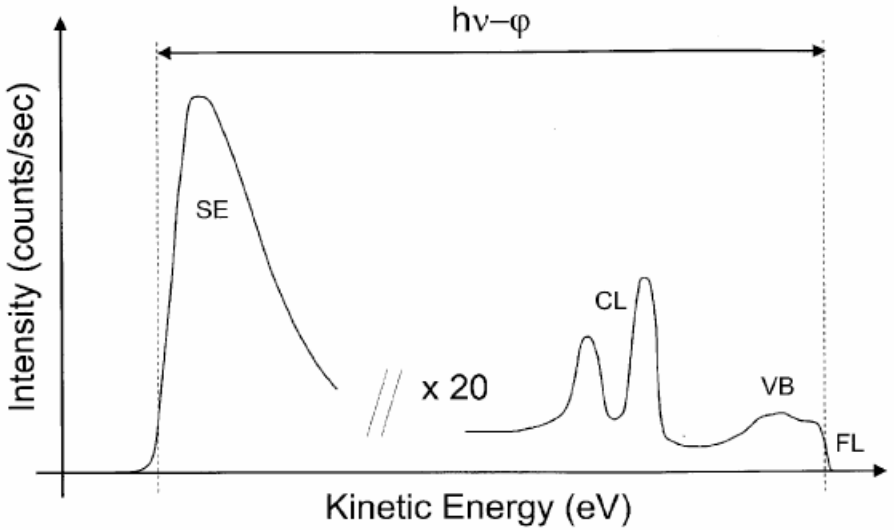

(a) total yield mode, i.e., collection of all emitted PEs;
(b) low pass filtering, i.e., collection of PEs with kinetic energies below a certain value;
(c) high pass filtering, i.e., collection of PEs with kinetic energies above a certain value;
(d) band pass filtering, i.e., collection of PEs within a certain energy window.

XAS mode

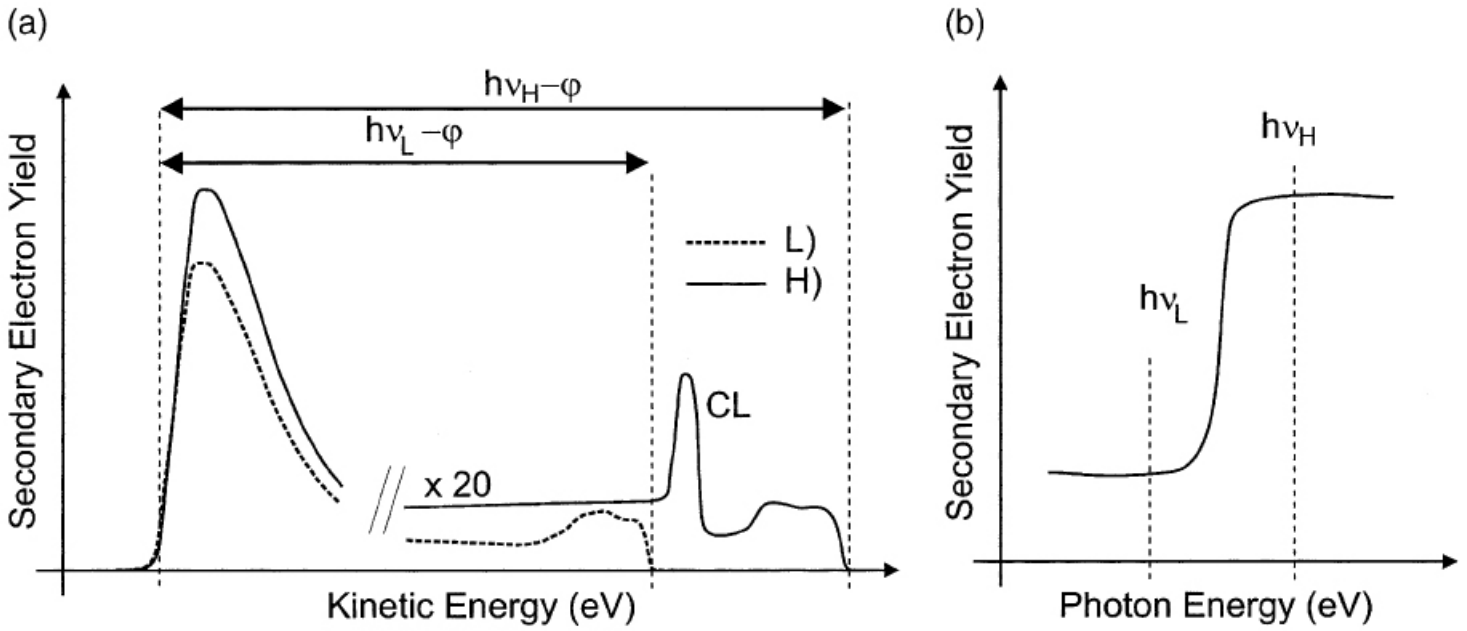

- Chemical sensitivity at threshold! (→ requires tunability of photons)
- Good for magnetic imaging
- Due to long IMFP attenuation al low KE → imaging buried layers and interfaces

XPS mode

XPS – mode: hν=const

hν in / e^- out

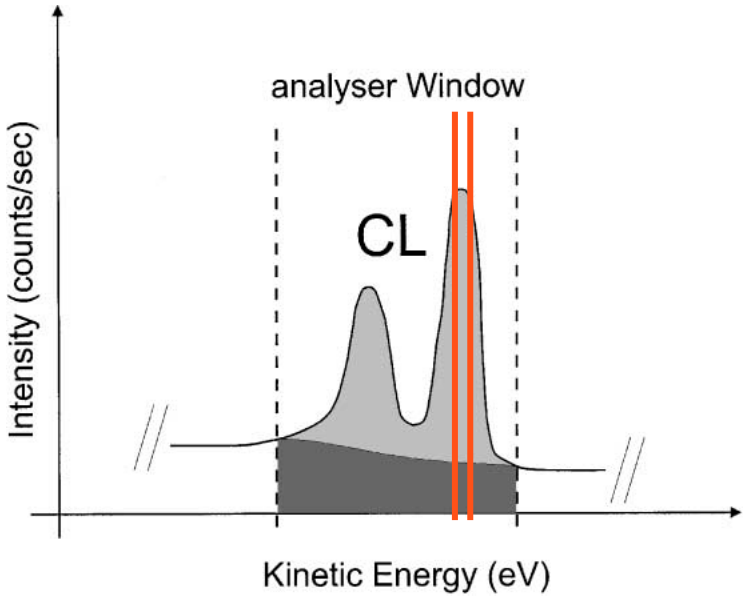

- Chemical sensitivity by measurement of BE
- Possibility of measuring SCLS
- High surface sensitivity
- Surface and chemical characterisation with LEEM PEEM instruments

Surface sensitivity

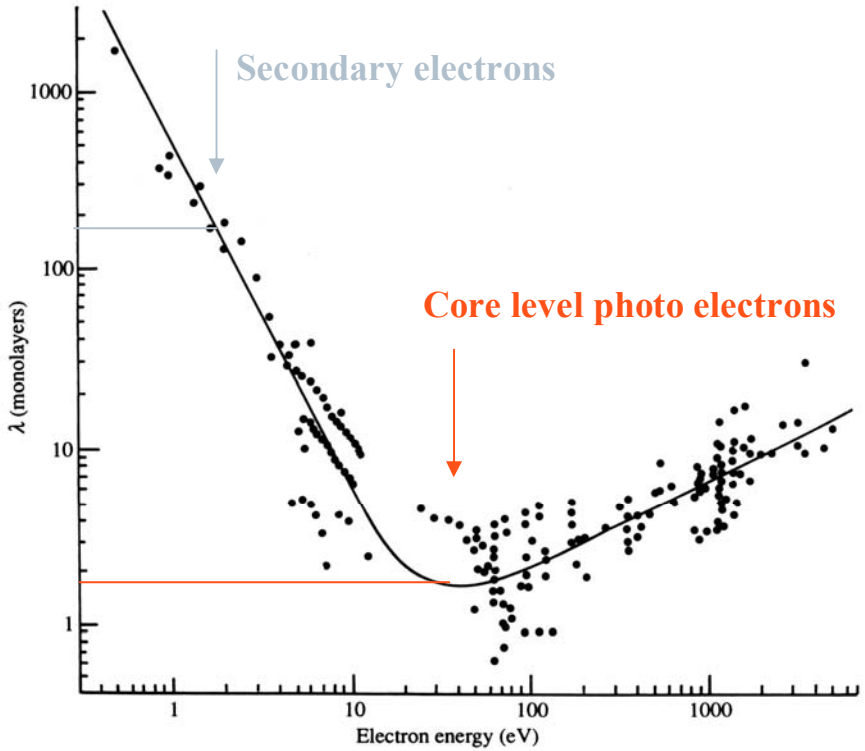

Inelastic mean free path
("universal curve")
determines sampling depth

reaction induced reorganisation of Au/Rh(110)

LEEM field of view 20 μm

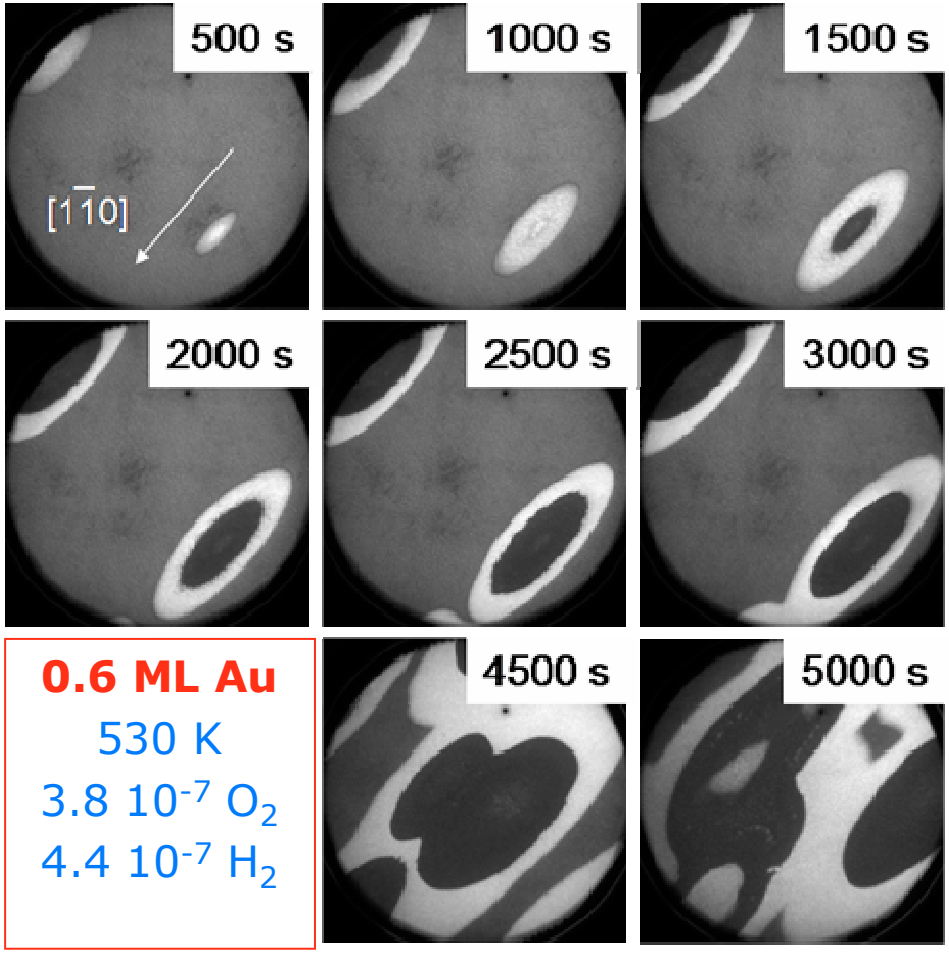

0.6 ML Au
530 K
3.8 10^{-7} O_2
4.4 10^{-7} H_2

XPEEM Au 4f

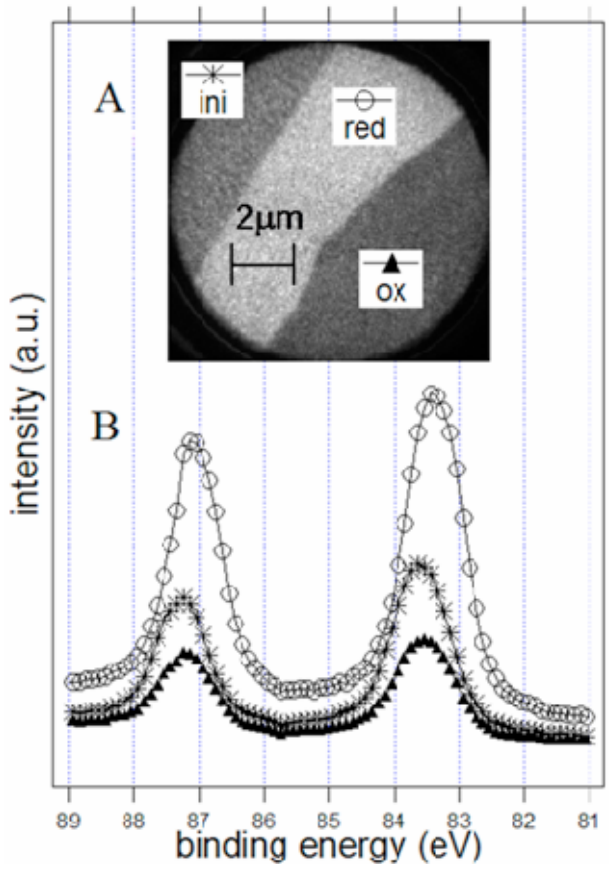

J. Am. Chem. Soc.; 127(7); 2351-2357 (2005).

reaction induced re0rganisation of Au/Rh(110) with micro-XPS and XPEEM

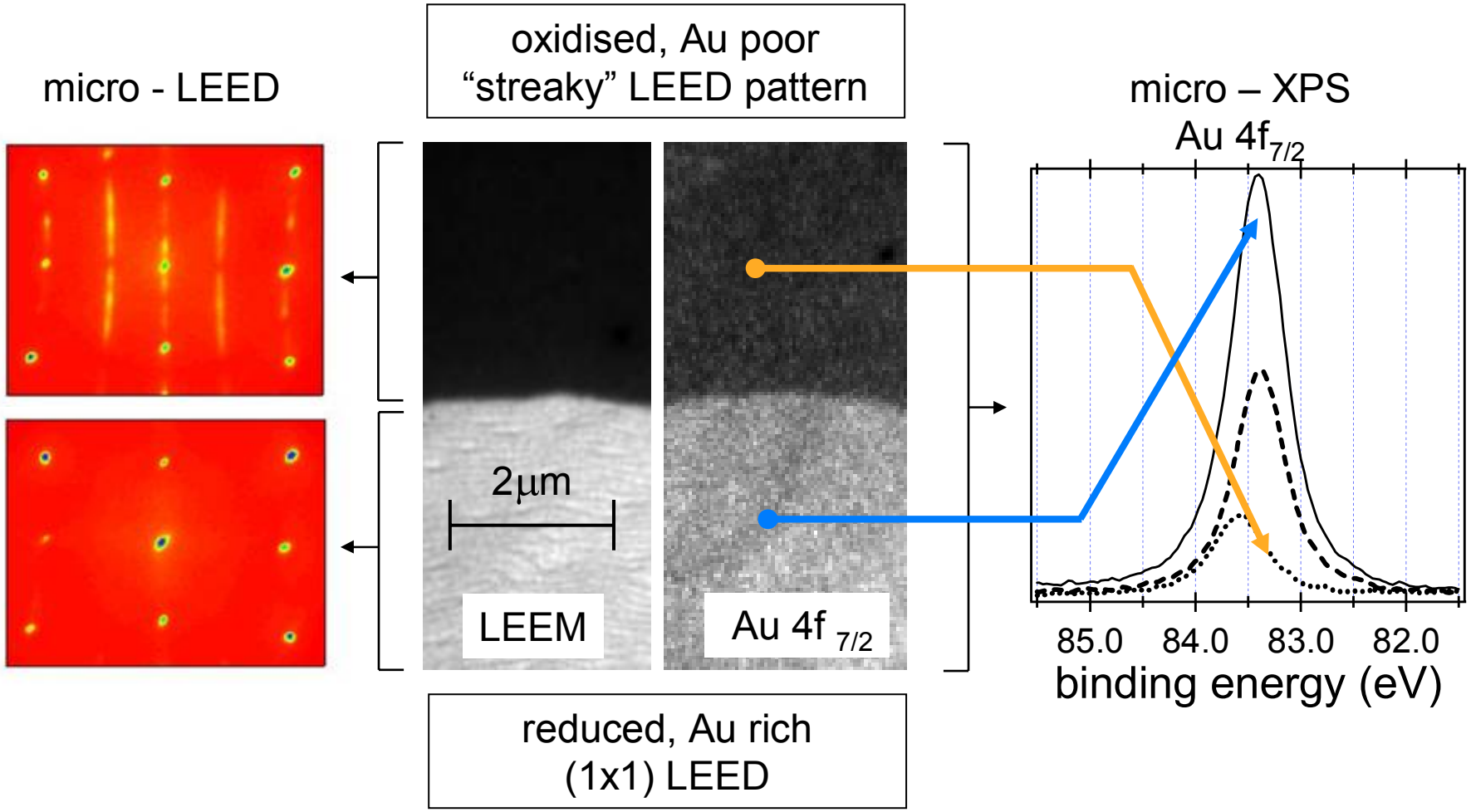

Reaction induced pattern formation with metal adsorbates on Rh(110) - XPEEM

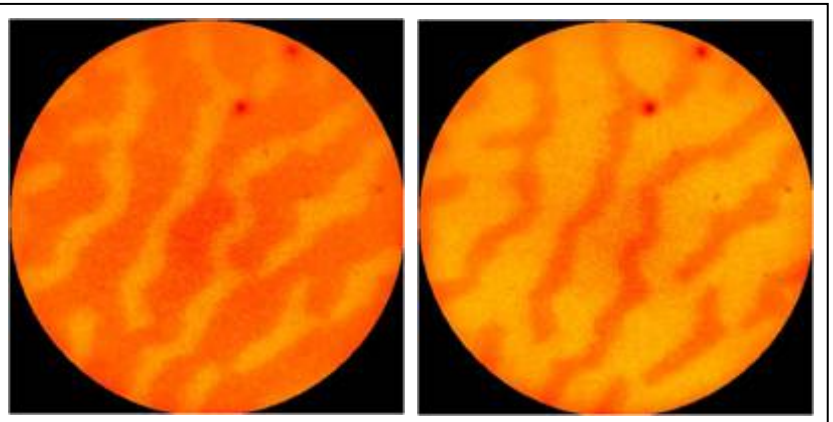

Pd 3d $_{3/2}$

Rh 3d $_{3/2}$

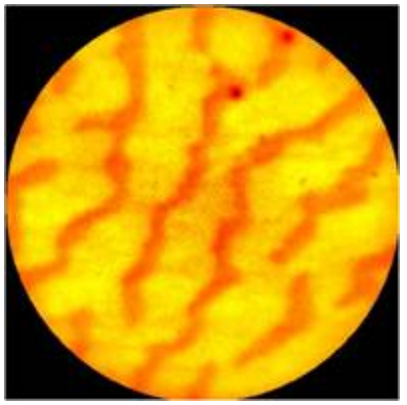

O 2p

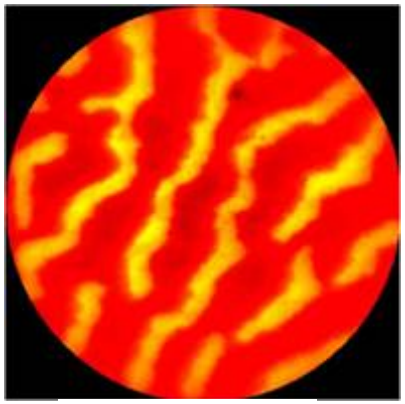

Au 4f $_{7/2}$

0.5 ML Pd
0.25 ML Au
670 K
3.8 10^{-7} O_2
1.4 10^{-7} H_2
XPEEM
fov 10 μm

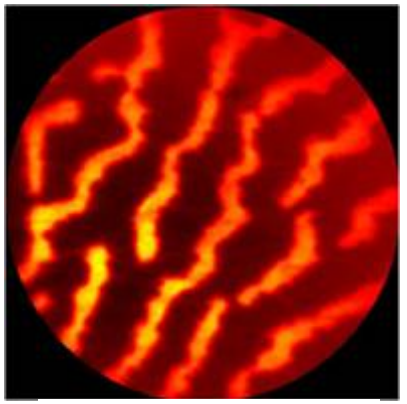

K.E. 1.2 eV

XMCD principles

- X-ray magnetic circular dichroism **XMCD** is the dependence of x-ray absorption on the relative orientation of the local magnetization and the polarization vector of the circularly polarized light

- In the case of ferromagnets (Ni, Fe, Co) **3d electrons** determine magnetic properties:

  $m_s = \langle N_{up} - N_{down} \rangle m_b$ for Co 1.64 m_b

  $m_o << m_s$ for Co 0.14 m

- We **PROBE** 3d elements by exciting 2p into unfilled 3d states
  - 2p → 3d channel dominant
  - White line intensity proportional to number of holes
  - Sum rules to determine m_s and m_o

XMCD principles

d band as detector for the spin

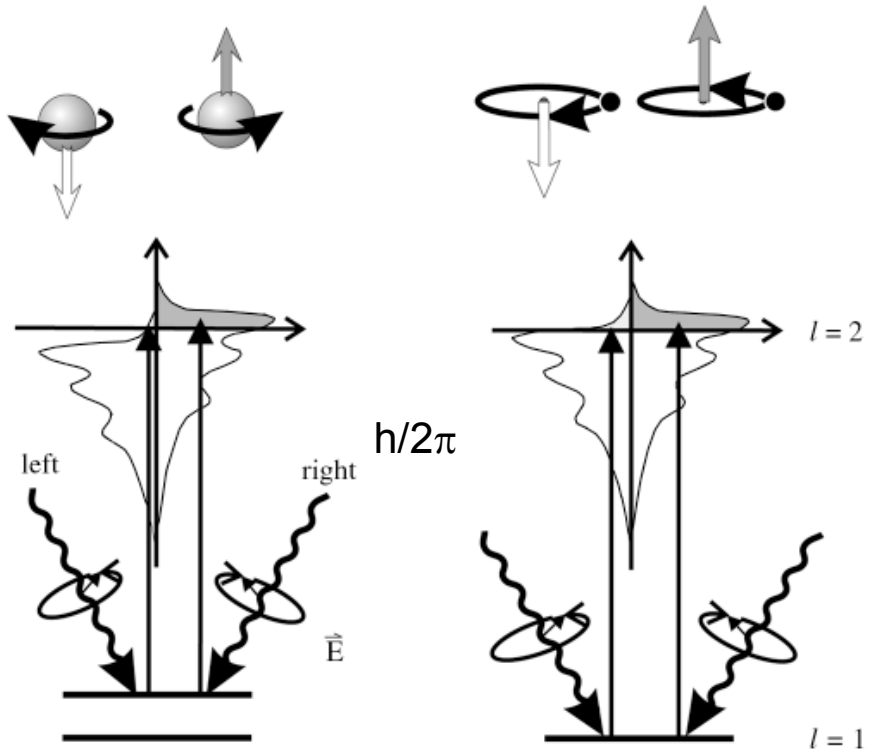

Opposite spin orbit coupling

$L_3 = l+s$

$L_2 = l-s$

J. Stöhr / Journal of Magnetism and Magnetic Materials 200 (1999) 470–497

Experimental Confirmation of the X-Ray Magnetic Circular Dichroism Sum Rules for Iron and Cobalt

C. T. Chen,[1] Y. U. Idzerda,[2] H.-J. Lin,[1,*] N. V. Smith,[1,†] G. Meigs,[1] E. Chaban,[1]
G. H. Ho,[3,*] E. Pellegrin,[1] and F. Sette[1,‡]

PRL 75, 152; 1995

SUM RULES

$$m_{\text{orb}} = -\frac{4\int_{L_3+L_2}(\mu_+ - \mu_-)\,d\omega}{3\int_{L_3+L_2}(\mu_+ + \mu_-)\,d\omega}(10 - n_{3d}), \quad (1)$$

$$m_{\text{spin}} = -\frac{6\int_{L_3}(\mu_+ - \mu_-)\,d\omega - 4\int_{L_3+L_2}(\mu_+ - \mu_-)\,d\omega}{\int_{L_3+L_2}(\mu_+ + \mu_-)\,d\omega} \times (10 - n_{3d})\left(1 + \frac{7\langle T_z\rangle}{2\langle S_z\rangle}\right)^{-1}, \quad (2)$$

$\langle T_z \rangle$ is the expectation value of the magnetic dipole operator

$\langle S_z \rangle$ is equal to half of m_{spin}

REFERENCES

B. T. Thole, P. Carra, F. Sette, and G. van der Laan, Phys. Rev. Lett. 68, 1943 (1992); P. Carra, B. T. Thole, M. Altarelli, and X.Wang, Phys. Rev. Lett. 70, 694 (1993), J.Stöhr et al, Phys. Rev. Lett. 75 (1995) 3748.

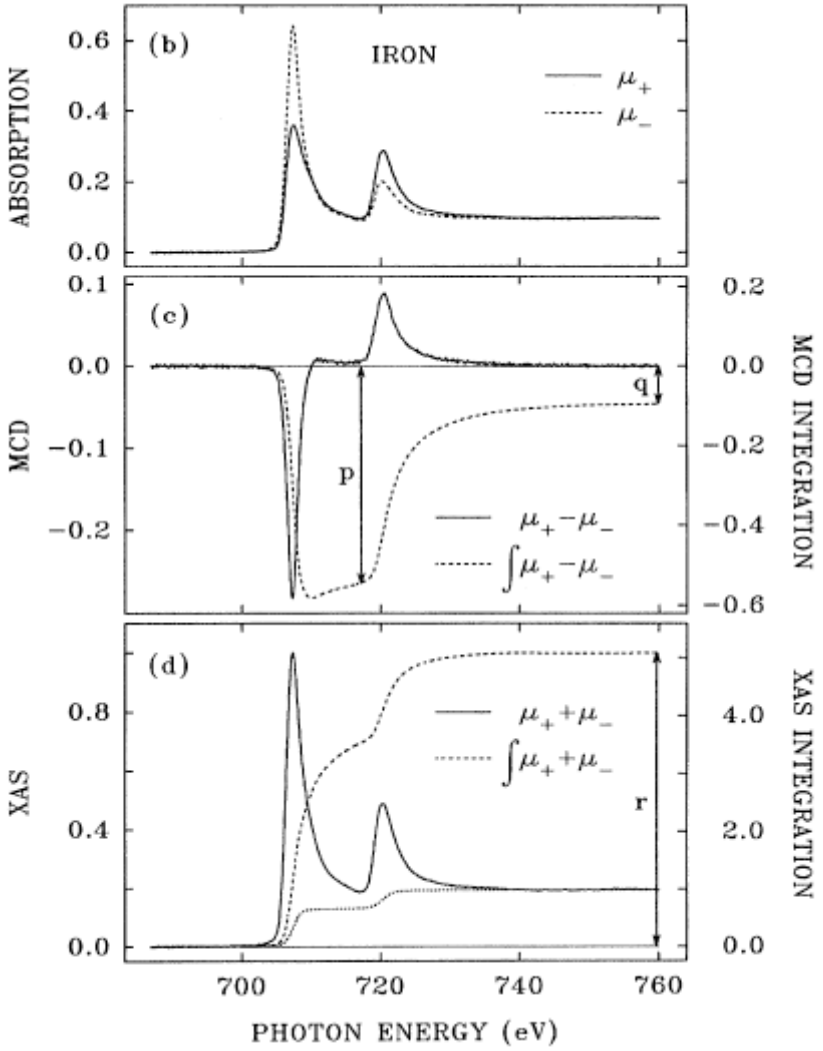

XMCD PEEM practical

- Quantitative technique that allows measuring spin and orbital magnetic moments
- Elemental sensitivity!
- Suitable for imaging applications with different techniques, i.e., XPEEM. TXM, SPEM
- XMCD image: $(I_- - I_+)/(I_- + I_+)$, where $I_{+,-}$ are the images acquired with positive and negative photon helicity
- effect is maximum when magnetisation parallel or anti-parallel to helicity vector

An example: Co/W(110)

XMCD = $(L_2-L_3)/(L_2+L_3)$

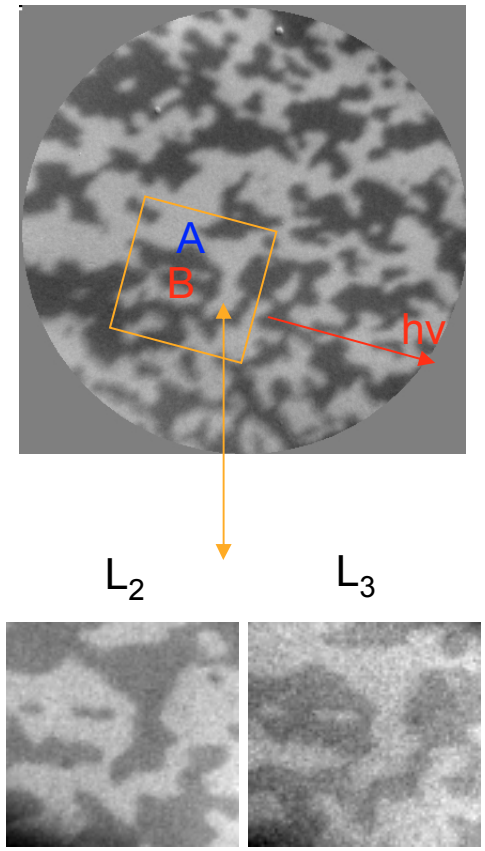

10 ML Co / W{110}

$m_{spin}=-(6p-4q)*(1-n_d)/r*(1/deg_{CP})$

$m_{orb}=-4/3*(1-n_d)*q/r*(1/deg_{CP})$

n_d[Co] = 7.51; deg_{CP}= degree of circular polarization

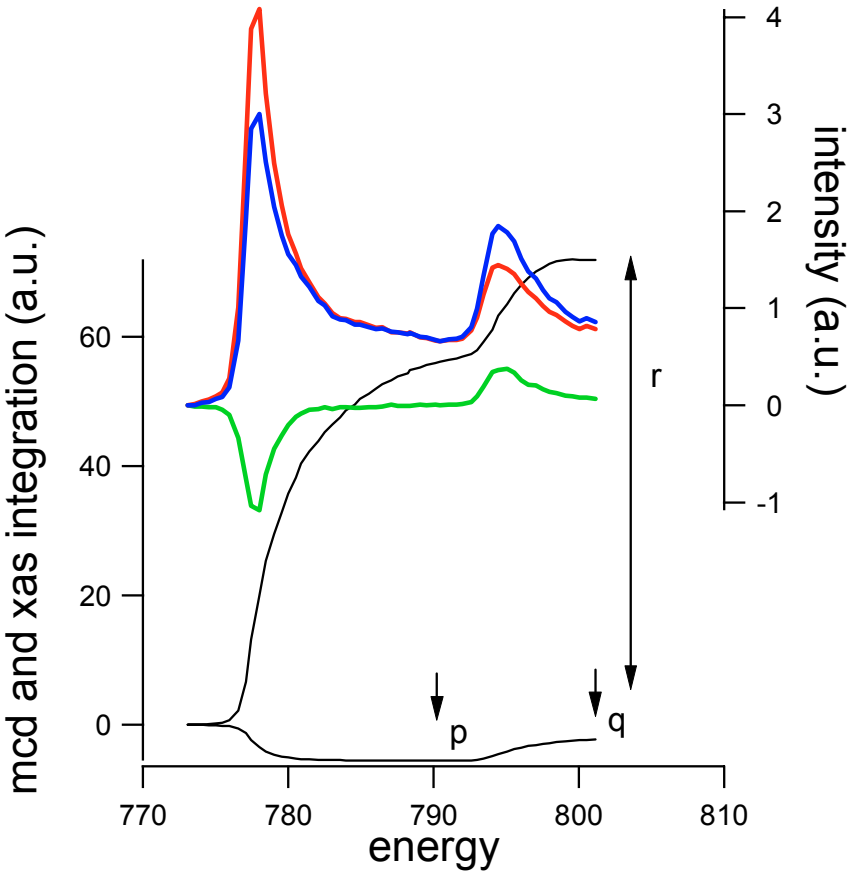

XMLD

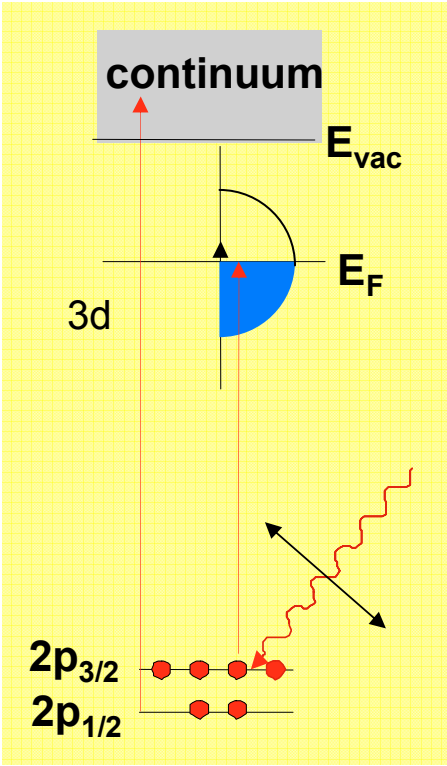

anti-ferromagnetic

absorption intensity at resonance

$$I(\vartheta,\theta,T) = a + b(3\cos^2\vartheta - 1)\langle Q_{zz}\rangle + c(3\cos^2\theta - 1)\langle M^2\rangle_T + d\sum_{i,j}\langle \hat{s}_i \cdot \hat{s}_j\rangle_T$$

Q_{zz} = quadrupole moment of charge, “linear dichroism”

ϑ is the angle of $\vec{E}$ with the crystallographic z axis.

2nd term determines XMLD effect

Θ is the angle between E and magnetic axis A

M reflects long range magnetic order

XMLD at max. for E ∥ A

Examples: XMCD and XMLD

Direct observation of the alignment of ferromagnetic spins by antiferromagnetic spins

F. Nolting*, A. Scholl*, J. Stöhr†, J. W. Seo‡§, J. Fompeyrine§, H. Siegwart§, J.-P. Locquet§, S. Anders*, J. Lüning†, E. E. Fullerton†, M. F. Toney†, M. R. Scheinfein‖ & H. A. Padmore*

Nature, 405 (2000), 767.

Figure 1 Images and local spectra from the antiferromagnetic and ferromagnetic layers for 1.2-nm Co on $LaFeO_3/SrTiO_3(001)$. **a**, Fe L-edge XMLD image; **b**, Co L-edge XMCD image. The contrast in the images arises from antiferromagnetic domains in $LaFeO_3$ (**a**) and ferromagnetic domains in Co (**b**) with in-plane orientations of the antiferromagnetic axis and ferromagnetic spins as indicated below the images. The spectra shown underneath were recorded in the indicated areas and illustrate the origin of the intensity contrast in the PEEM images.

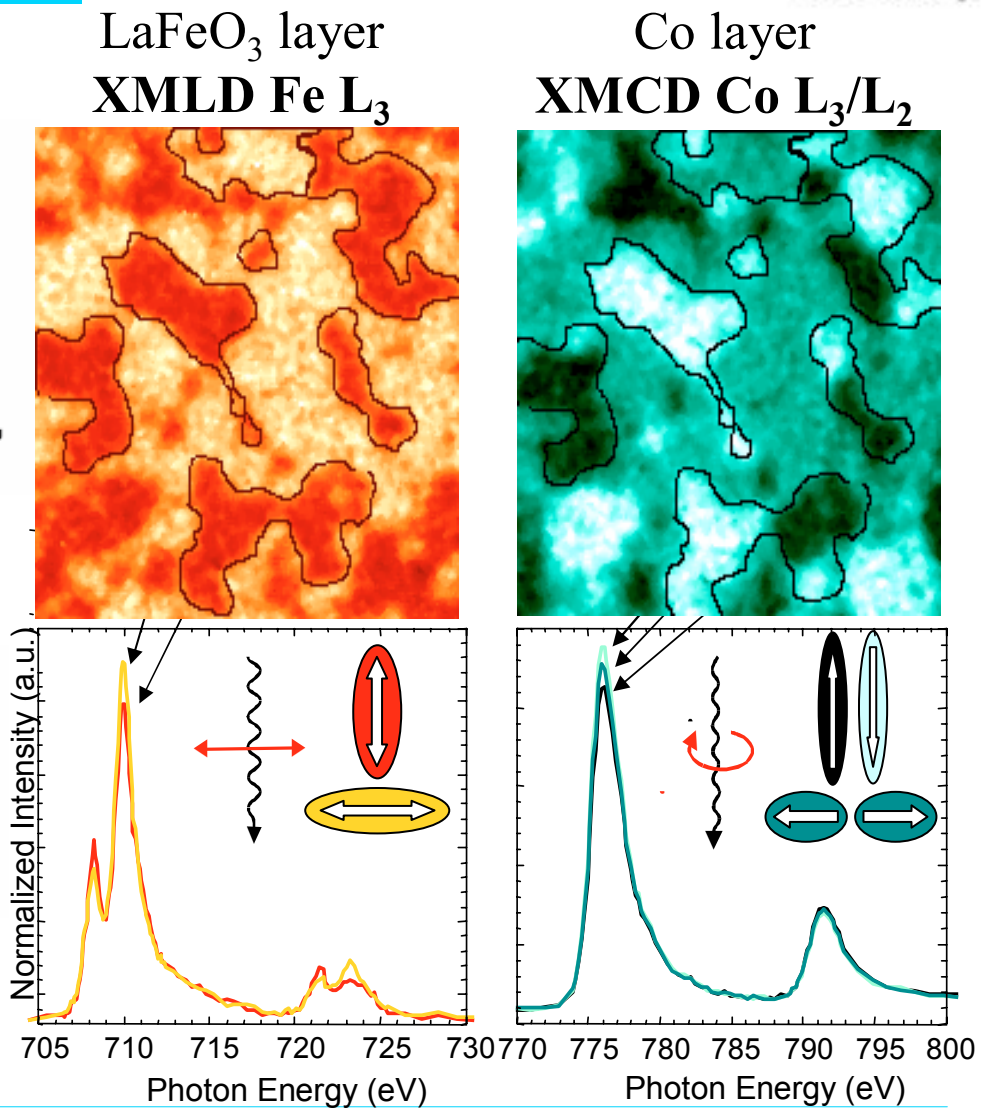

Examples – MnAs/GaAs

MnAs for spin injection into GaAs at room temperature?

Problem: strain-induced phase coexistence between ferromagnetic and paramagnetic phase around room temperature

α T< ≈ 40 °C NiAs (hexagonal) ferromagnetic
β MnP (orthorhombic) paramagnetic
γ T > 125 °C NiAs (hexagonal) paramagnetic

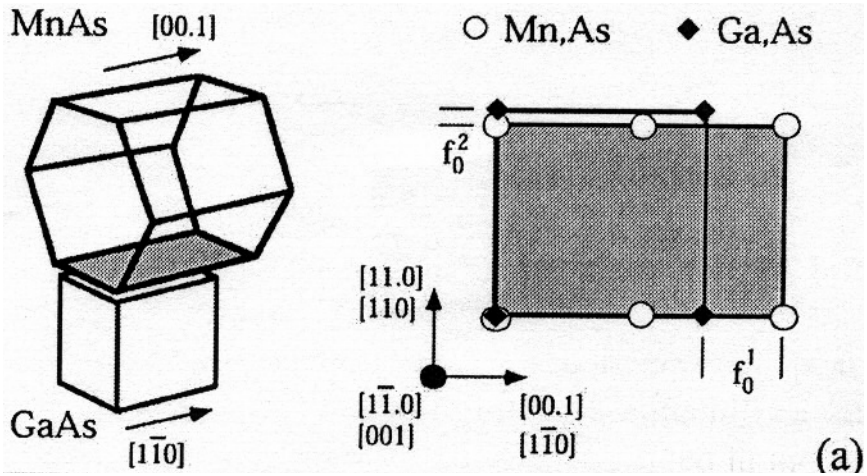

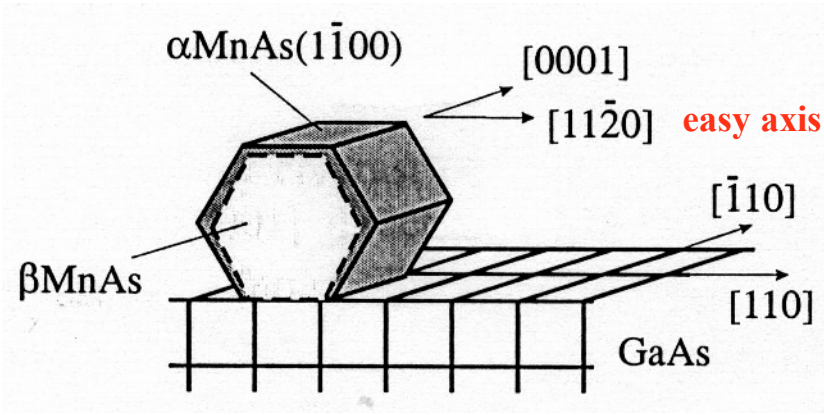

α MnAs / GaAs(100) $f_0^2 = 7.7\%$

from L. Daeweritz et al ≥ 1999

Examples – MnAs/GaAs

MnAs on GaAs(100)

Thickness dependence of magnetic domain structure

Room temperature

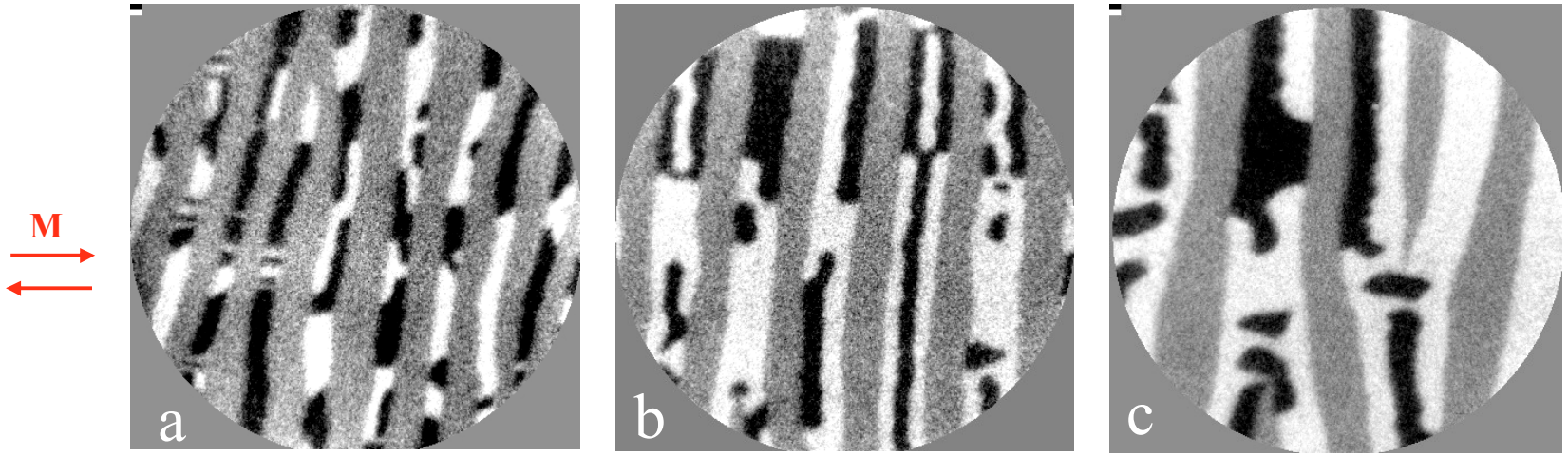

120 nm **180 nm** **300 nm**

Field of view 5 μm diameter

Examples – magnetic bits

domain configuration and vortex in rings

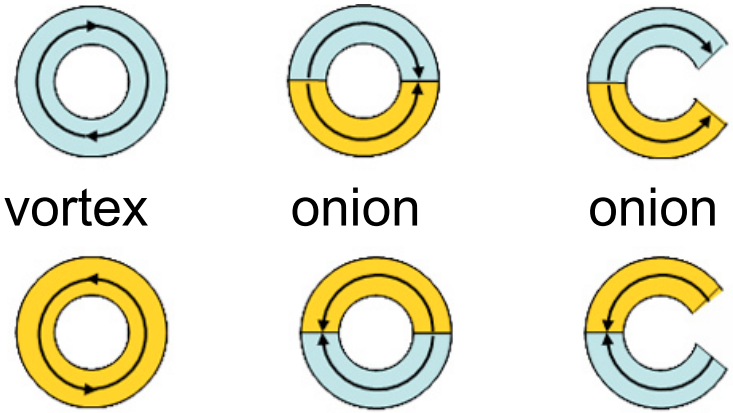

ring shaped Co polycrystalline elements

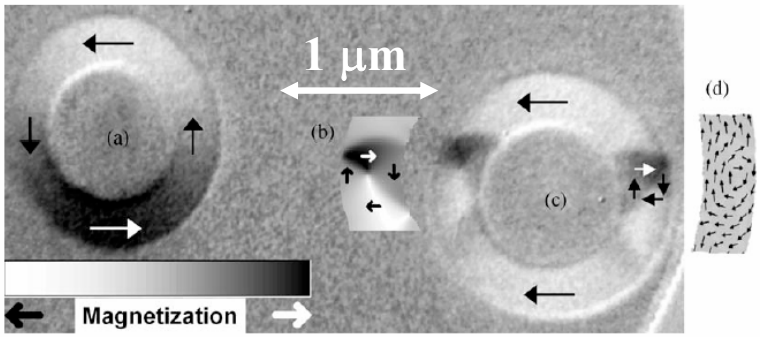

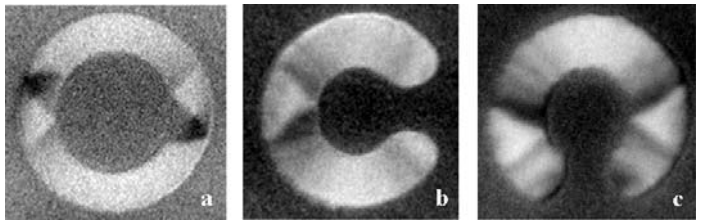

(a) Vortex state
(b) Vortex head to head walls (simulation)
(c) Onion state
(d) Magnetisation configuration of (c)

M.Klaui, C.A.F. Vaza, W.Wernsdorfer, E.Bauer, S.Cherifi, S.Heun, A.Locatelli, G.Faini, E.Cambril, L.J. Heydermanf, J.A.C. Bland

Examples - nanostructures

The ability to control growth processes on semiconductor surfaces will play a crucial role for the development of novel technologies such as high-density data storage, nanoscopic sensors, and even q-bits for quantum computing. The **self-organisation** of the matter provides an elegant efficient method for producing ordered arrays of nanostructures, potentially able to surpass lithography in speed and quality. Here, self-organized semiconductor surfaces have been used as large-area templates for the growth of Co magnetic nanostructures.

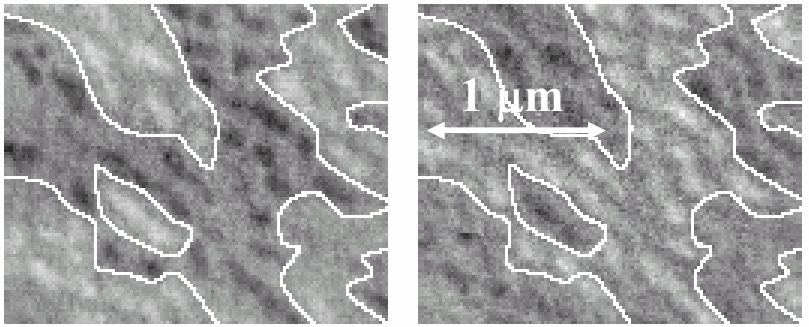

XMCD imaging of Co quantum dots

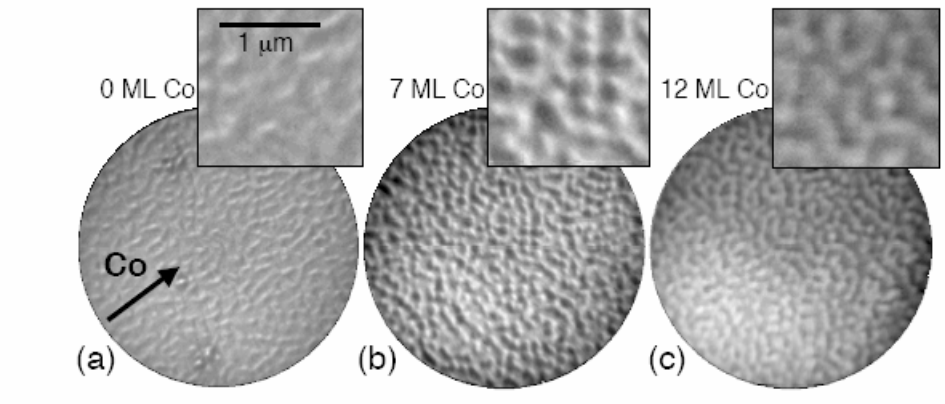

in situ growth of self – organized magnetic nano-particles

The microscope available at Elettra's **Nano-spectroscopy beamline** allows full characterisation of quantum dot magnetic nanostructures. The images on the left demonstrate that the morphology of the Co deposit is dictated by the surface templates. The images shown above show that magnetic contrast appears only in the Co rich regions. The dots are elongated along the direction perpendicular to Co deposition and this promotes an uniaxial magnetic anisotropy. Magnetic correlation between the dots is present, giving rise to magnetic domain patterns in the Co films.

Phys. Rev. B 71, 214422 (2005).

Magnetic imaging at Elettra

The "Nanospectroscopy" beamline

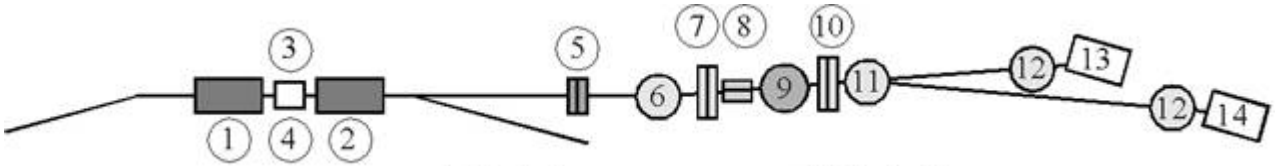

1: Section 1.1
2: Section 1.2
3: Modulator
4: Source
5: Pinhole
6: Toroidal mirror
7: Entrance Slit (horiz.)
8: Entrance Slit (vert.)
9: Monochromator
10: Exit-slit
11: Deflection mirror
12: Refocussing pair
13: SPELEEM
14: Second branch end station

Source: Variable Polarization, helical undulator

Monochromator: Wide spectral range
Medium spectral resolution

Spot: High photon flux density on sample
Small variable spot size (~μm)
Homogeneous illumination

Microscope: SPELEEM (Elmitec)

Helicity fast switching at SLS

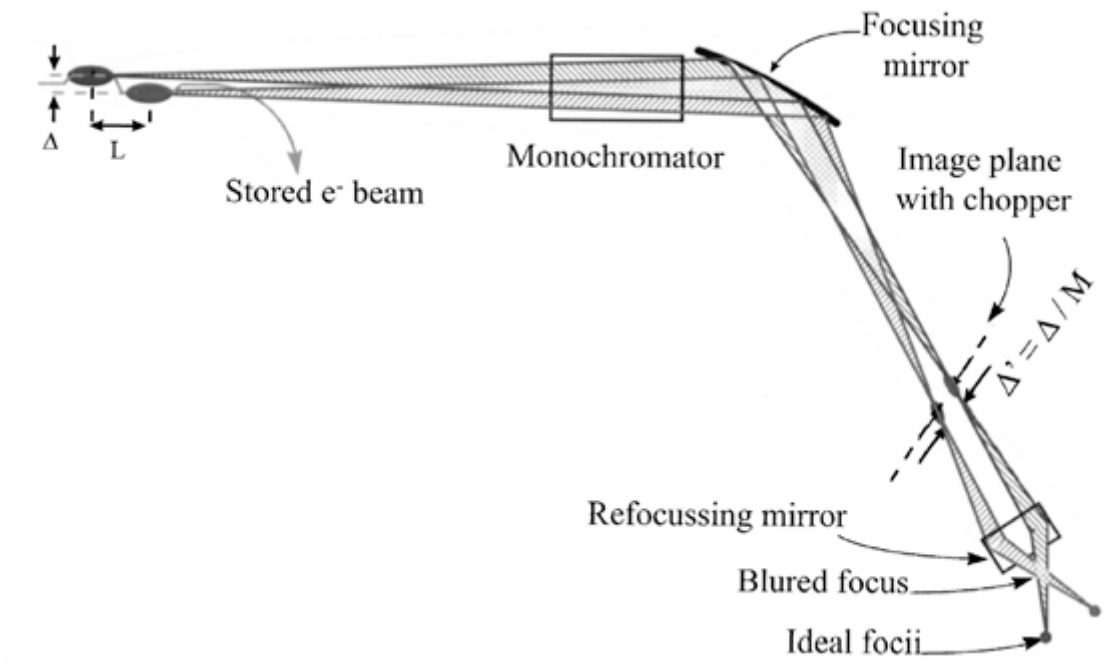

ELSEVIER

Surface Science 480 (2001) 173–179

SURFACE SCIENCE

www.elsevier.nl/locate/susc

A beamline for time resolved photoelectron microscopy on magnetic materials at the Swiss light source

C. Quitmann [a,*], U. Flechsig [a], L. Patthey [a], T. Schmidt [a], G. Ingold [a], M. Howells [b], M. Janousch [a], R. Abela [a]

[a] *Paul Scherrer Institut, Swiss Light Source, CH-5232 Villigen-PSI, Switzerland*
[b] *Advanced Light Source, Lawrence Berkeley National Laboratory, Berkeley, CA 94720, USA*

Our design also uses two IDs located one behind the other, but as a novel feature the optical paths for the two photon beams overlap almost completely. Therefore it is sufficient to use a single set of relatively small mirrors to accept and guide both photon beams. The operation principle is shown in Fig. 1. Two IDs are located in the same straight section one behind the other. Each of them acts as a radiation source. Using steerer magnets located before, between, and after the IDs a small parallel offset is created in the electron orbit. This causes a separation of the two source points by L in longitudinal and by Δ in transverse direction. The IDs are set to the same photon energy, but to opposite helicity. A focusing mirror having demagnification $1/M$, located behind the monochromator images these two source points onto the image plane. Here the two sources cause two images separated by $\Delta' = \Delta/M$. A mechanical chopper, located in the image plane, alternatively blocks one of the two photon beams. This arrangement now provides a beam of photons with switchable helicity. The two photon beams can be overlapped on the sample using a single refocussing mirror. This mirror creates two images of the two source points, but in front of the ideal focus, the two photon beams overlap in a blurred focus, see Fig. 1. As long as the source separation Δ is small, this blurred focus is close to the ideal focus and its diameter is comparable to that of the ideal focus.

Time resolved experiments

Stroboscopic experiments combine high lateral resolution of PEEM with high time resolution, taking advantage of pulsed nature of synchrotron radiation

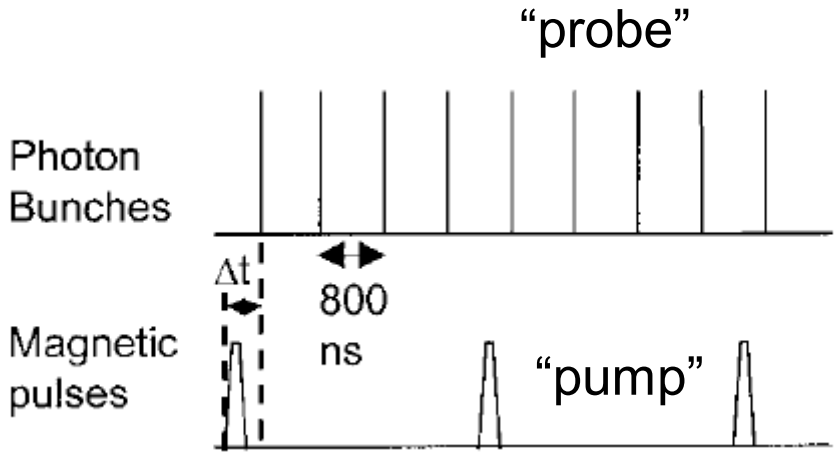

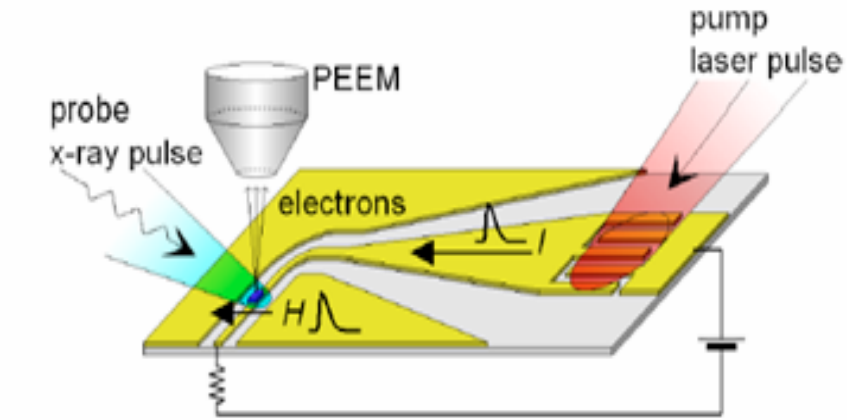

FIG. 1. Photon pulses (top) of about 100 ps length arrive on the sample every 800 ns. A magnetic pulse is given every 3.2 μs (middle), with a width of 20 ns and a delay Δt with respect to one of the photon pulses. For the other three photon pulses, a negative pulse of 80 V and 80 ns width is given to the grid of the PEEM (bottom) to block most of the secondary electrons.

Vogel et al, APL 82, 2299 (2003).

Setup for "pump & probe"

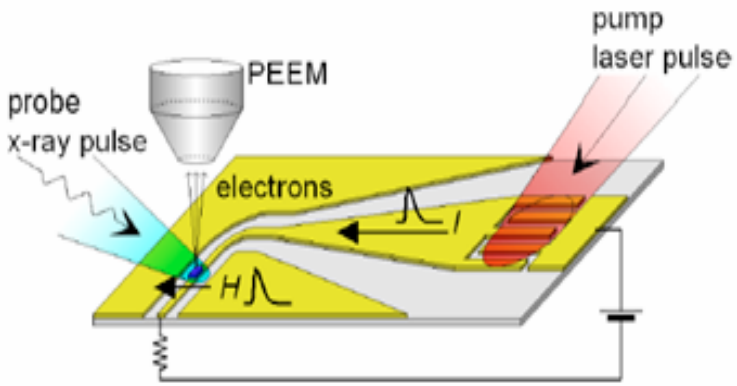

FIG. S1. Schematic of the experimental arrangement.

Experimental Setup

The experimental setup is shown in Fig. S1. Fast in-plane field pulses on top of a waveguide are derived from current pulses, launched in a photoconductive switch. The switch is activated by pulses from a Ti:Sapphire laser of 800 nm wavelength at 125 MHz repetition rate. The current pulses have a fast rising edge below the resolution of this experiment and an amplitude of about 15 mT. They decay exponentially with a time constant of about 300 ps. The sample is probed by soft x-rays from the bending magnet beamline 7.3.1.1 of the Advanced Light Source (ALS). The spot size is about 30x30 μm^2. The x-rays are pulsed at a repetition rate of 3.05 MHz, phase-locked to the laser pulses. At this frequency every 41st pump field pulse is probed. The time evolution of the state of the sample is measured by varying the electronic delay between the pump pulse and the probe pulse with an accuracy of about 20 ps. The laser frequency limits the scan range to 0-8 ns. The time resolution of the measurement is determined by the length of the x-ray pulse of about 70 ps.

Choe et Al, Science, 304 (2004), 420

Quantitative Analysis of Magnetic Excitations in Landau Flux-Closure Structures Using Synchrotron-Radiation Microscopy

J. Raabe,[1,*] C. Quitmann,[1] C. H. Back,[2] F. Nolting,[1] S. Johnson,[1] and C. Buehler[1]

The time dependent magnetization is described by the phenomenological Landau-Lifshitz-Gilbert equation

$$\frac{d}{dt}\vec{M} = -\gamma_0 \vec{M} \times \vec{H}_{\text{eff}} + \frac{\alpha}{M}\left(\vec{M} \times \frac{d}{dt}\vec{M}\right).$$

The first term describes the precession of the magnetization $\vec{M}$ about the total effective field $\vec{H}_{\text{eff}}$. The second term describes the relaxation back into the equilibrium state using the dimensionless damping parameter α.

xmcd

t_i-t_0

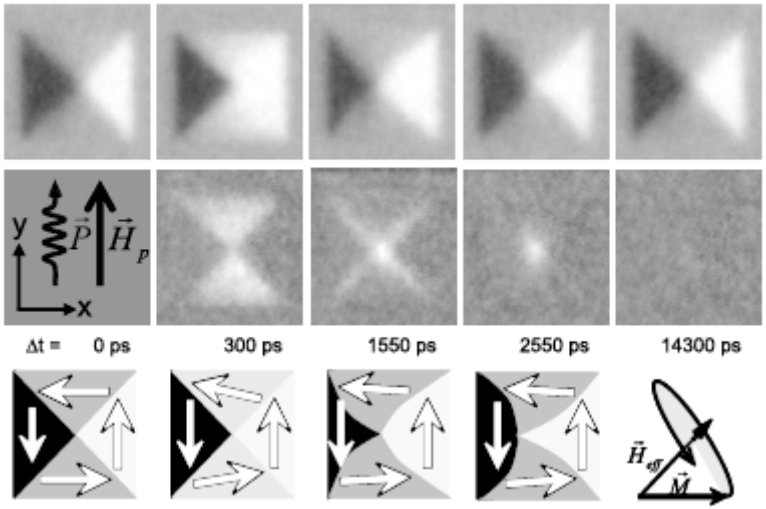

PRL 94, 217204 (2005)

MEASUREMENT OF:

- Vortex displacement (max 750 nm)
- Domain wall displacement and buldging
- Vortex velocity (~ 700 m/s)
- Quantitative time-dependent magnetisation
- Fourier analysis

torque $\vec{T} = -\gamma_0 \vec{M} \times \vec{H}_{\text{eff}}$

Imaging domain dynamics

Vortex Core–Driven Magnetization Dynamics

S.-B. Choe,[1*] Y. Acremann,[2] A. Scholl,[1] A. Bauer,[1,2,3] A. Doran,[1] J. Stöhr,[2] H. A. Padmore[1]

Time-resolved x-ray imaging shows that the magnetization dynamics of a micron-sized pattern containing a ferromagnetic vortex is determined by its handedness, or chirality. The out-of-plane magnetization in the nanometer-scale vortex core induces a three-dimensional handedness in the planar magnetic structure, leading to a precessional motion of the core parallel to a subnanosecond field pulse. The core velocity was an order of magnitude higher than expected from the static susceptibility. These results demonstrate that handedness, already well known to be important in biological systems, plays an important role in the dynamics of microscopic magnets.

Science, 304 (2004), 420

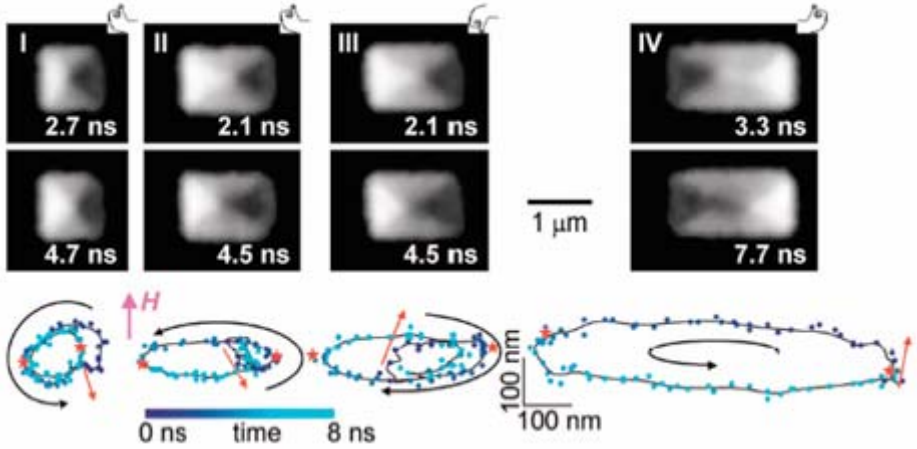

Opposite rotation is caused by direction of vortex core magnetization, i.e. chirality